electronics

Article

Monopulse Radar Target Detection in the Case of Main-Lobe Cover Jamming

Lei Wang [1,2], Qiliang Zhang [1] and Pengfei Wan [1,3,*]

[1] Air Defence and Anti Missile College, Air Force Engineering University, Xi'an 710051, China
[2] Unit 93688 of People's Liberation Army, Tianjin 300202, China
[3] National Laboratory of Radar Signal Processing, Xidian University, Xi'an 710071, China
* Correspondence: wanpengfei@stu.xidian.edu.cn

Abstract: Radar is known as the "eye" of modern warfare and plays a pivotal role in warfare, but the detection performance of radar systems is seriously affected by main-lobe cover jamming. To solve this problem, a radar target detection method based on four-channel monopulse radar is proposed in this paper. This method designed a spatial filter for main-lobe jamming cancellation, which could cancel the main-lobe jamming while keeping the target signal power unchanged, ensuring that the Electronic counter-countermeasure Improvement Factors (*EIF*) of the filtered signal always reach the maximum value to improve the target detection performance of monopulse radar. The Monte Carlo simulation results showed that the algorithm in this paper outperformed the conventional Main-Lobe Cancellation (MLC) algorithm in terms of EIFs and detection performance.

Keywords: main-lobe cover jamming; spatial filter; MLC

check for updates

Citation: Wang, L.; Zhang, Q.; Wan, P. Monopulse Radar Target Detection in the Case of Main-Lobe Cover Jamming. *Electronics* **2022**, *11*, 3539. https://doi.org/10.3390/electronics11213539

Academic Editor: Federico Alimenti

Received: 2 October 2022
Accepted: 25 October 2022
Published: 30 October 2022

Publisher's Note: MDPI stays neutral with regard to jurisdictional claims in published maps and institutional affiliations.

Copyright: © 2022 by the authors. Licensee MDPI, Basel, Switzerland. This article is an open access article distributed under the terms and conditions of the Creative Commons Attribution (CC BY) license (https://creativecommons.org/licenses/by/4.0/).

1. Introduction

Monopulse technology is a technique that is widely used in current radar systems [1], but with the development of electronic jamming techniques, various styles of intentional and unintentional jamming make the electromagnetic environment of the monopulse radar increasingly complex. Among them, main-lobe cover jamming is a common jamming style, which is usually used by enemies accompanying a jammer or in towed jammer casts to cover the fighters, bombers, and other moving targets. The jamming enters the receiver from the radar antenna's main lobe and maintains a small angle with the target. At this time, the jamming obtains the main lobe gain of the radar directional diagram, and the jamming power is much larger than the target signal power, resulting in masking jamming of the radar, so target detection cannot be achieved. The traditional methods used to suppress side-lobe jamming, such as low side-lobe antennas [2,3], Side-Lobe Cancellation [4–8] (SLC), and Side-Lobe Blanking [9–11] (SLB), have become invalid because of the small angle between the jammer and the target. Adaptive Digital Beam Forming (ADBF) technology can cause a serious loss of the target signal due to the zero trap formed at the jamming angle. Therefore, main-lobe cover jamming severely limits the detection performance of monopulse radar.

At present, there are five main mature techniques for main-lobe jamming suppression, e.g., ADBF based on Blocking Matrix Preprocessing (BMP) [12–15] and Eigen-projection Matrix Preprocessing (EMP) [16–18], which can realize adaptive jamming cancellation from spatial filtering. However, the BMP-based method relies on the accurate information of the jamming angle, and the EMP-based method has the problem that the eigenvector corresponding to the main-lobe jamming is difficult to determine. The algorithm performance will be seriously degraded when the jamming angle is not estimated accurately or the eigenvector is not calculated appropriately. The second technique is the jamming suppression method of four-channel monopulse MLC [19,20], which is similar to the SLC technique, canceling the main-lobe jamming by receiving signals of the azimuth difference channel, pitch difference channel, and double difference channel. The third is the jamming

suppression method based on multistatic radar [21,22], which mainly uses the angle between the jammer and different base stations to locate the jamming to further suppress the main-lobe jamming, but this method requires phase synchronization between different base stations, which is difficult to implement. The fourth is the jamming suppression method based on polarization cancellation [23], which is mainly based on the polarization slow change of the radar antenna in the scanned airspace and the polarization filtering of the received echo signal to suppress the main-lobe jamming, but this method can only suppress single-polarization main-lobe jamming. The fifth is the suppression method based on jamming perception [24,25], which mainly distinguishes the jamming from the target signal through the difference in the characteristics of the jamming and the target echo, but the premise of this method is that the target echo signal and the jamming are already separated or only one jamming exists in the echo signal, so it is limited in practical applications.

In summary, radar main-lobe cover jamming is a classical problem in the radar field, which seriously affects the combat effectiveness of radar systems, and the current jamming suppression methods cannot solve this problem. Inspired by the idea of building an optimization model and using boundary conditions to solve the optimal solution in literature [26,27], a target detection algorithm was proposed based on monopulse radar under the background of main-lobe cover jamming, which performs inter-beam spatial filtering on the received signal of the monopulse radar under the criterion of maximizing the *EIF* so as to suppress the main-lobe jamming. The subsequent content of this paper is organized as follows: Section 2 establishes the signal model, Section 3 introduces the relevant principles of the algorithm, Section 4 performs the simulation verification, Section 5 is the discussion, and Section 6 is the conclusion.

2. Signal Model

For the four-channel monopulse radar with the number of vertical and horizontal array elements as N_e, N_a, respectively, the four channels are the sum channel, pitch difference channel, azimuth difference channel, and double difference channel. The main-lobe cover jamming is $\boldsymbol{S}_j$, the target signal is $\boldsymbol{S}_t$, the number of echo points received by the radar is M, and the monopulse antenna received by the signal model can be expressed as

$$\boldsymbol{X} = \boldsymbol{A}\boldsymbol{S} + \boldsymbol{N}$$

$$\begin{bmatrix} g_{\Sigma j}s_{j1} + g_{\Sigma t}s_{t1} + n_{\Sigma 1} & g_{\Sigma j}s_{j2} + g_{\Sigma t}s_{t2} + n_{\Sigma 2} & \cdots & g_{\Sigma j}s_{jM} + g_{\Sigma t}s_{tM} + n_{\Sigma M} \\ g_{\Delta_e j}s_{j1} + g_{\Delta_e t}s_{t1} + n_{\Delta_e 1} & g_{\Delta_e j}s_{j2} + g_{\Delta_e t}s_{t2} + n_{\Delta_e 2} & \cdots & g_{\Delta_e j}s_{jM} + g_{\Delta_e t}s_{tM} + n_{\Delta_e M} \\ g_{\Delta_a j}s_{j1} + g_{\Delta_a t}s_{t1} + n_{\Delta_a 1} & g_{\Delta_a j}s_{j2} + g_{\Delta_a t}s_{t2} + n_{\Delta_a 2} & \cdots & g_{\Delta_a j}s_{jM} + g_{\Delta_a t}s_{tM} + n_{\Delta_a M} \\ g_{\Delta_\Delta j}s_{j1} + g_{\Delta_\Delta t}s_{t1} + n_{\Delta_\Delta 1} & g_{\Delta_\Delta j}s_{j2} + g_{\Delta_\Delta t}s_{t2} + n_{\Delta_\Delta 2} & \cdots & g_{\Delta_\Delta j}s_{jM} + g_{\Delta_\Delta t}s_{tM} + n_{\Delta_\Delta M} \end{bmatrix}. \quad (1)$$

where

$$\boldsymbol{A} = \begin{bmatrix} g_{\Sigma j} & g_{\Sigma t} \\ g_{\Delta_e j} & g_{\Delta_e t} \\ g_{\Delta_a j} & g_{\Delta_a t} \\ g_{\Delta_\Delta j} & g_{\Delta_\Delta t} \end{bmatrix} \quad (2)$$

is the jamming and target signal gain matrix; the four elements in the first column of the matrix represent the gain value of the four radar channels that correspond to the jamming from top to bottom, and the four elements in the second column of the matrix represent the gain value of the four radar channels that correspond to the target signal from top to bottom.

$$\boldsymbol{S} = \begin{bmatrix} \boldsymbol{s}_j \\ \boldsymbol{s}_t \end{bmatrix} = \begin{bmatrix} s_{j1} & s_{j2} & \cdots & s_{jM} \\ s_{t1} & s_{t2} & \cdots & s_{tM} \end{bmatrix} \quad (3)$$

is the jamming and target signal matrix. $\boldsymbol{S}_j$ is the row vector composed of the first row of elements of the matrix, representing the jamming received by the radar. $\boldsymbol{S}_t$ is the row

vector composed of the second row of elements of the matrix, representing the target signal received by the radar.

$$\boldsymbol{N} = \begin{bmatrix} n_{\Sigma 1} & n_{\Sigma 2} & \cdots & n_{\Sigma \mathrm{M}} \\ n_{\Delta_{\mathrm{e}} 1} & n_{\Delta_{\mathrm{e}} 2} & \cdots & n_{\Delta_{\mathrm{e}} \mathrm{M}} \\ n_{\Delta_{\mathrm{a}} 1} & n_{\Delta_{\mathrm{a}} 2} & \cdots & n_{\Delta_{\mathrm{a}} \mathrm{M}} \\ n_{\Delta_{\Delta} 1} & n_{\Delta_{\Delta} 2} & \cdots & n_{\Delta_{\Delta} \mathrm{M}} \end{bmatrix} \tag{4}$$

is the receiver noise matrix; the four row vectors composed of the elements in the first row to the fourth row represent the noise signals in the four respective channels of the receiver.

For ease of representation, set

$$\boldsymbol{X} = \begin{bmatrix} \boldsymbol{x}_{\Sigma} \\ \boldsymbol{x}_{\Delta_{\mathrm{e}}} \\ \boldsymbol{x}_{\Delta_{\mathrm{a}}} \\ \boldsymbol{x}_{\Delta_{\Delta}} \end{bmatrix} = \begin{bmatrix} \boldsymbol{x}_{\Sigma \mathrm{j}} \\ \boldsymbol{x}_{\Delta_{\mathrm{e}} \mathrm{j}} \\ \boldsymbol{x}_{\Delta_{\mathrm{a}} \mathrm{j}} \\ \boldsymbol{x}_{\Delta_{\Delta} \mathrm{j}} \end{bmatrix} + \begin{bmatrix} \boldsymbol{x}_{\Sigma \mathrm{t}} \\ \boldsymbol{x}_{\Delta_{\mathrm{e}} \mathrm{t}} \\ \boldsymbol{x}_{\Delta_{\mathrm{a}} \mathrm{t}} \\ \boldsymbol{x}_{\Delta_{\Delta} \mathrm{t}} \end{bmatrix} + \begin{bmatrix} \boldsymbol{n}_{\Sigma} \\ \boldsymbol{n}_{\Delta_{\mathrm{e}}} \\ \boldsymbol{n}_{\Delta_{\mathrm{a}}} \\ \boldsymbol{n}_{\Delta_{\Delta}} \end{bmatrix}, \tag{5}$$

where $\boldsymbol{x}_{\Sigma}$, $\boldsymbol{x}_{\Delta_{\mathrm{e}}}$, $\boldsymbol{x}_{\Delta_{\mathrm{a}}}$, and $\boldsymbol{x}_{\Delta_{\Delta}}$ represent the received signals of the sum channel, pitch difference channel, azimuth difference channel, and double difference channel respectively.

3. Algorithm Principle

3.1. Principle of Cell Average Constant False Alarm Rate (CA-CFAR) Detection

In the actual radar signal processing, it is difficult to find a suitable threshold for target detection due to the large fluctuation of the jamming. Constant False Alarm Rate (CFAR) detection is a set of techniques to provide predictable detection and false alarms for radars in a jamming environment, which can dynamically adjust the detection threshold according to the magnitude of jamming power so that the radar has stable detection performance, also known as "adaptive threshold detection "or "automation-detection". The CA-CFAR algorithm is one of the most common CFAR algorithms; Figure 1 shows the principle block diagram of the CA-CFAR algorithm [28].

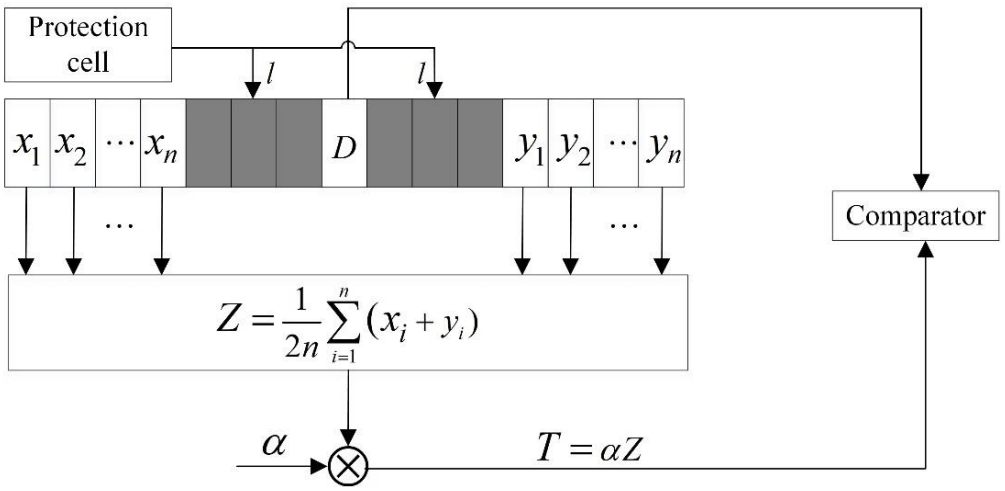


Figure 1. The principle of the CA-CFAR algorithm.

In Figure 1, D is the amplitude of the signal of the cell to be detected; take l protection cells on each side of the cell to be detected to prevent the problem of inaccurate noise level estimation caused by the energy leakage of the target signal through the protection cells. Therefore, the signal amplitude of the protected cells is not included during noise power estimation. Then, n reference cells $x_i(i = 1, 2 \cdots n)$ and $y_i(i = 1, 2 \cdots n)$ are taken to estimate the background noise power Z of the cell to be detected. Next, the estimated

background noise Z is multiplied by the threshold coefficient α to obtain the threshold T. Finally, the threshold T and the signal amplitude D of the cell to be detected are input into the comparator for comparison. When the signal amplitude of the cell to be detected is greater than the threshold value T, the target is determined to be present, otherwise, there is no target.

For the Gaussian distribution model of noise jamming, the probability density based on the square law detector obeys an exponential distribution, assuming that the jamming is independently and identically distributed, and the jamming power of the I and Q channels is $\sigma^2/2$, the probability density function is

$$f_x = \frac{1}{\sigma^2}\exp(-\frac{x}{\sigma^2}). \tag{6}$$

From Figure 1, the noise power estimated from the reference cells is

$$Z = \frac{1}{2n}\sum_{i=1}^{n}(x_i + y_i), \tag{7}$$

and then the estimated detection threshold T at the cell to be detected is

$$T = \alpha Z = \frac{\alpha}{2n}\sum_{i=1}^{n}(x_i + y_i). \tag{8}$$

From (6) and (8), the probability density distribution of the detection threshold T is

$$f_T = \frac{1}{(2n-1)!}\left(\frac{2n}{\alpha\sigma^2}\right)^{2n} T^{2n-1}\exp\left(-\frac{2nT}{\alpha\sigma^2}\right). \tag{9}$$

From the Neyman–Pearson criterion, the corresponding false alarm rate at the estimated detection threshold is given by

$$P_{fa} = \exp\left(-\frac{T}{\sigma^2}\right), \tag{10}$$

and the false alarm rate is obtained by integrating T

$$P_{fa} = \left(1 + \frac{\alpha}{2n}\right)^{-2n}. \tag{11}$$

Therefore, for a given false alarm rate, the threshold coefficient can be solved from (12) as

$$\alpha = 2n(P_{fa}^{-1/2n} - 1). \tag{12}$$

Then, from (8) and (12), the estimated detection threshold is

$$T = (P_{fa}^{-1/2n} - 1)\sum_{i=1}^{n}(x_i + y_i). \tag{13}$$

3.2. The ECCM Improvement Factors

EIF was proposed by S.L. Johston in 1974, which is an important index to measure the degree of improvement of the anti-jamming performance of radar systems by anti-jamming measures [29], usually expressed by the ratio of Signal-to-Jamming Ratio (SJR) with anti-jamming measures and without anti-jamming measures,

$$EIF = \frac{SJR}{SJR_0}. \tag{14}$$

where, SJR represents SJR with anti-jamming measures and SJR_0 represents SJR without jamming measures.

However, in practice, it is difficult to separate the jamming from the noise, so in this paper, the Signal-to-Jamming-plus-Noise Ratio ($SJNR$) is used instead of SJR to calculate the EIF,

$$EIF = \frac{SJNR}{SJNR_0}. \tag{15}$$

where, $SJNR$ represents $SJNR$ with anti-jamming measures and $SJNR_0$ represents $SJNR$ without jamming measures.

3.3. Principle of the MLC Algorithm

For the two-dimensional planar array, the longitudinal and transverse array elements are N_e and N_a; the array element are half-wavelength spaced, and the beam gains in the direction of the pitch angle θ_e and azimuth angle θ_a can be decomposed into the product of the corresponding one-dimensional pitch and one-dimensional azimuth monopulse antenna gains in the form of

$$g_\Sigma(\theta_e, \theta_a) = g_{\Sigma_{\theta ep,Ne}}(\theta_e) g_{\Sigma_{\theta ap,Na}}(\theta_a), \tag{16}$$

$$g_{\Delta_e}(\theta_e, \theta_a) = g_{\Delta_{\theta ep,Ne}}(\theta_e) g_{\Sigma_{\theta ap,Na}}(\theta_a), \tag{17}$$

$$g_{\Delta_a}(\theta_e, \theta_a) = g_{\Sigma_{\theta ep,Ne}}(\theta_e) g_{\Delta_{\theta ap,Na}}(\theta_a), \tag{18}$$

$$g_{\Delta_\Delta}(\theta_e, \theta_a) = g_{\Delta_{\theta ep,Ne}}(\theta_e) g_{\Delta_{\theta ap,Na}}(\theta_a). \tag{19}$$

where $g_\Sigma(\theta_e, \theta_a)$,$g_{\Delta_e}(\theta_e, \theta_a)$,$g_{\Delta_a}(\theta_e, \theta_a)$, and $g_{\Delta_\Delta}(\theta_e, \theta_a)$ denote the respective beam gains of the sum beam, pitch difference beam, azimuth difference beam, and double difference beam of the planar array in the pitch angle θ_e and azimuth angle θ_a.$g_{\Sigma_{\theta ep,Ne}}(\theta_e)$,$g_{\Delta_{\theta ep,Ne}}(\theta_e)$ are the sum beam and difference beam gains of the uniform linear array placed longitudinally with the number of array elements N_e and the array elements half-wavelength spaced at pitch angle θ_e, and $g_{\Sigma_{\theta ap,Na}}(\theta_a)$, $g_{\Delta_{\theta ap,Na}}(\theta_a)$ are the sum and difference beam gains of the uniform linear array placed laterally with the number of elements N_a and the array elements half-wavelength spaced at the azimuth angle θ_a.

When the jamming $\boldsymbol{s}_j$ originates from the pitch angle θ_{ej} and azimuth angle θ_{aj}, the target signal $\boldsymbol{s}_t$ originates from the pitch angle θ_{et} and azimuth angle θ_{at}; the mixed signals of the jamming, target, and noise output from the four channels of the monopulse system can be expressed as

$$\boldsymbol{x}_\Sigma = g_\Sigma(\theta_{ej}, \theta_{aj})\boldsymbol{s}_j + g_\Sigma(\theta_{et}, \theta_{at})\boldsymbol{s}_t + \boldsymbol{n}_\Sigma, \tag{20}$$

$$\boldsymbol{x}_{\Delta_e} = g_{\Delta_e}(\theta_{ej}, \theta_{aj})\boldsymbol{s}_j + g_{\Delta_e}(\theta_{et}, \theta_{at})\boldsymbol{s}_t + \boldsymbol{n}_{\Delta_e}, \tag{21}$$

$$\boldsymbol{x}_{\Delta_a} = g_{\Delta_a}(\theta_{ej}, \theta_{aj})\boldsymbol{s}_j + g_{\Delta_a}(\theta_{et}, \theta_{at})\boldsymbol{s}_t + \boldsymbol{n}_{\Delta_a}, \tag{22}$$

$$\boldsymbol{x}_{\Delta_\Delta} = g_{\Delta_\Delta}(\theta_{ej}, \theta_{aj})\boldsymbol{s}_j + g_{\Delta_\Delta}(\theta_{et}, \theta_{at})\boldsymbol{s}_t + \boldsymbol{n}_{\Delta_\Delta}. \tag{23}$$

Since the main-lobe jamming power is much higher than the target signal power, the target signal is completely covered by the jamming, and target detection is not possible. The researchers proposed the monopulse antenna inter-beam MLC technique; from (20)–(23), the signals in the four channels of the monopulse radar consist of the same signal components, so the pitch dimension jamming in the sum channel can be eliminated by the signal of the pitch difference channel. The azimuth dimension jamming in the sum channel can be eliminated by the signal of the azimuth difference channel, and the jamming in the pitch difference channel and azimuth difference channel can be eliminated by the double difference channel signal, and then target detection can be carried out. Figure 2 shows the principle of the MLC algorithm [19].

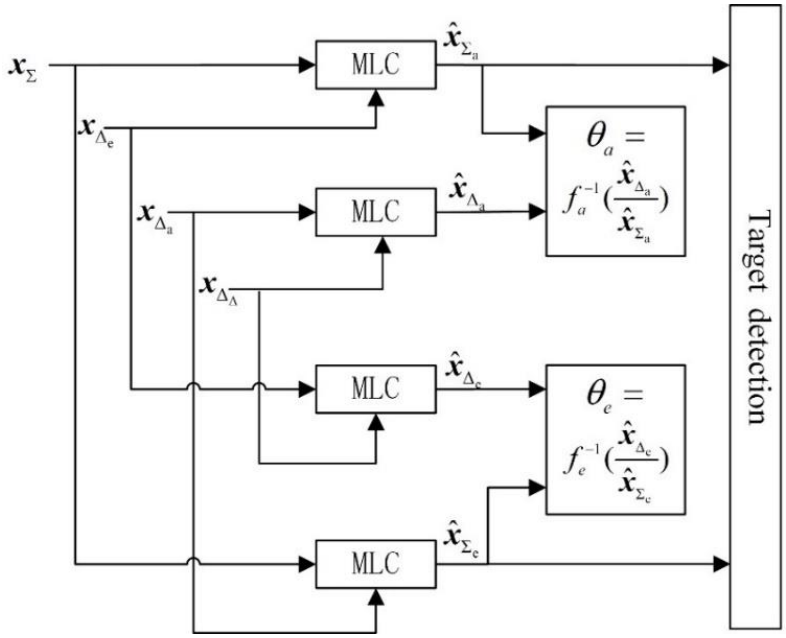


Figure 2. The principle of the MLC algorithm.

The output signal of each channel of the monopulse antenna after MLC can be expressed as

$$\hat{\boldsymbol{x}}_{\Sigma_e} = \boldsymbol{x}_\Sigma - v_a \boldsymbol{x}_{\Delta_a}, \tag{24}$$

$$\hat{\boldsymbol{x}}_{\Delta_e} = \boldsymbol{x}_{\Delta_e} - v_a \boldsymbol{x}_{\Delta_\Delta}, \tag{25}$$

$$\hat{\boldsymbol{x}}_{\Sigma_a} = \boldsymbol{x}_\Sigma - v_e \boldsymbol{x}_{\Delta_e}, \tag{26}$$

$$\hat{\boldsymbol{x}}_{\Delta_a} = \boldsymbol{x}_{\Delta_a} - v_e \boldsymbol{x}_{\Delta_\Delta}, \tag{27}$$

$$v_a = \frac{1}{2}\frac{\mathrm{E}[\boldsymbol{x}_\Sigma \circ \bar{\boldsymbol{x}}_{\Delta_a}]}{\mathrm{E}[\boldsymbol{x}_{\Delta_a} \circ \bar{\boldsymbol{x}}_{\Delta_a}]} + \frac{1}{2}\frac{\mathrm{E}[\boldsymbol{x}_{\Delta_e} \circ \bar{\boldsymbol{x}}_{\Delta_\Delta}]}{\mathrm{E}[\boldsymbol{x}_{\Delta_\Delta} \circ \bar{\boldsymbol{x}}_{\Delta_\Delta}]}, \tag{28}$$

$$v_e = \frac{1}{2}\frac{\mathrm{E}[\boldsymbol{x}_\Sigma \circ \bar{\boldsymbol{x}}_{\Delta_e}]}{\mathrm{E}[\boldsymbol{x}_{\Delta_e} \circ \bar{\boldsymbol{x}}_{\Delta_e}]} + \frac{1}{2}\frac{\mathrm{E}[\boldsymbol{x}_{\Delta_a} \circ \bar{\boldsymbol{x}}_{\Delta_\Delta}]}{\mathrm{E}[\boldsymbol{x}_{\Delta_\Delta} \circ \bar{\boldsymbol{x}}_{\Delta_\Delta}]}. \tag{29}$$

where "$\mathrm{E}(\cdot)$" represents the average of all of the elements of the vector, "$\circ$" represents the Hadamard product between vectors, and "$\overline{(\cdot)}$" represents conjugate vectors.

After MLC processing, target detection can be carried out in the $\hat{\boldsymbol{x}}_{\Sigma_e}$ channel for azimuthal dimension jamming cancellation or in the $\hat{\boldsymbol{x}}_{\Sigma_a}$ channel for pitch dimension jamming cancellation. When the radar has no anti-jamming measures, the power of the target signal, jamming, and noise in the sum channel is

$$P_{\Sigma t0} = \boldsymbol{x}_{\Sigma t}\boldsymbol{x}_{\Sigma t}^{\mathrm{H}} = (\mathrm{g}_{\Sigma t})^2 \boldsymbol{s}_t \boldsymbol{s}_t^{\mathrm{H}}, \tag{30}$$

$$P_{\Sigma j0} = \boldsymbol{x}_{\Sigma j}\boldsymbol{x}_{\Sigma j}^{\mathrm{H}} = (\mathrm{g}_{\Sigma j})^2 \boldsymbol{s}_j \boldsymbol{s}_j^{\mathrm{H}}, \tag{31}$$

$$P_{\Sigma n0} = \boldsymbol{n}_\Sigma \boldsymbol{n}_\Sigma^{\mathrm{H}}. \tag{32}$$

From (30)–(32), *SJNR* without anti-jamming measures is

$$SJNR_0 = \frac{P_{\Sigma t0}}{P_{\Sigma j0} + P_{\Sigma n0}} = \frac{(\mathrm{g}_{\Sigma t})^2 \boldsymbol{s}_t \boldsymbol{s}_t^{\mathrm{H}}}{(\mathrm{g}_{\Sigma j})^2 \boldsymbol{s}_j \boldsymbol{s}_j^{\mathrm{H}} + \boldsymbol{n}_\Sigma \boldsymbol{n}_\Sigma^{\mathrm{H}}}, \tag{33}$$

and after MLC processing, the $\hat{\boldsymbol{x}}_{\Sigma_e}$ channel can be expressed as

$$\boldsymbol{x}_{\Sigma_e} = \boldsymbol{x}_{\Sigma} - v_a \boldsymbol{x}_{\Delta_a} = (g_{\Sigma t} - v_a g_{\Delta_a t})\boldsymbol{s}_t + (g_{\Sigma j} - v_a g_{\Delta_a j})\boldsymbol{s}_j + (\boldsymbol{n}_{\Sigma} - \boldsymbol{n}_{\Delta_a}). \tag{34}$$

With the use of the MLC algorithm after azimuth dimension jamming cancellation, the power of the target signal, jamming, and noise in the $\boldsymbol{x}_{\Sigma_e}$ channel are

$$P_{\Sigma_e t} = (g_{\Sigma t} - v_a g_{\Delta_a t})^2 \boldsymbol{s}_t \boldsymbol{s}_t^H, \tag{35}$$

$$P_{\Sigma_e j} = (g_{\Sigma j} - v_a g_{\Delta_a j})^2 \boldsymbol{s}_j \boldsymbol{s}_j^H, \tag{36}$$

$$P_{\Sigma_e n} = (\boldsymbol{n}_{\Sigma} - \boldsymbol{n}_{\Delta_a})(\boldsymbol{n}_{\Sigma} - \boldsymbol{n}_{\Delta_a})^H. \tag{37}$$

The *SJNR* of the MLC algorithm after azimuth dimension jamming cancellation in the $\boldsymbol{x}_{\Sigma_e}$ channel is

$$SJNR_{\mathrm{MLC_e}} = \frac{(g_{\Sigma t} - v_a g_{\Delta_a t})^2 \boldsymbol{s}_t \boldsymbol{s}_t^H}{(g_{\Sigma j} - v_a g_{\Delta_a j})^2 \boldsymbol{s}_j \boldsymbol{s}_j^H + (\boldsymbol{n}_{\Sigma} - \boldsymbol{n}_{\Delta_a})(\boldsymbol{n}_{\Sigma} - \boldsymbol{n}_{\Delta_a})^H}. \tag{38}$$

Then, the *EIF* of the MLC algorithm after azimuth dimension jamming cancellation is

$$EIF_{\mathrm{MLC_e}} = \frac{SJNR_{\mathrm{MLC_e}}}{SJNR_0} = \frac{(g_{\Sigma t} - v_a g_{\Delta_a t})^2 [(g_{\Sigma j})^2 \boldsymbol{s}_j \boldsymbol{s}_j^H + \boldsymbol{n}_{\Sigma} \boldsymbol{n}_{\Sigma}^H]}{(g_{\Sigma t})^2 [(g_{\Sigma j} - v_a g_{\Delta_a j})^2 \boldsymbol{s}_j \boldsymbol{s}_j^H + (\boldsymbol{n}_{\Sigma} - \boldsymbol{n}_{\Delta_a})(\boldsymbol{n}_{\Sigma} - \boldsymbol{n}_{\Delta_a})^H]}. \tag{39}$$

Similarly, the *SJNR* of the MLC algorithm after pitch dimension jamming cancellation in the $\boldsymbol{x}_{\Sigma_a}$ channel is

$$SJNR_{\mathrm{MLC_a}} = \frac{(g_{\Sigma t} - v_e g_{\Delta_e t})^2 \boldsymbol{s}_t \boldsymbol{s}_t^H}{(g_{\Sigma j} - v_e g_{\Delta_e j})^2 \boldsymbol{s}_j \boldsymbol{s}_j^H + (\boldsymbol{n}_{\Sigma} - \boldsymbol{n}_{\Delta_e})(\boldsymbol{n}_{\Sigma} - \boldsymbol{n}_{\Delta_e})^H}, \tag{40}$$

and the *EIF* of the MLC algorithm after pitch dimension jamming cancellation is

$$EIF_{\mathrm{MLC_a}} = \frac{SJNR_{\mathrm{MLC_a}}}{SJNR_0} = \frac{(g_{\Sigma t} - v_e g_{\Delta_e t})^2 [(g_{\Sigma j})^2 \boldsymbol{s}_j \boldsymbol{s}_j^H + \boldsymbol{n}_{\Sigma} \boldsymbol{n}_{\Sigma}^H]}{(g_{\Sigma t})^2 [(g_{\Sigma j} - v_e g_{\Delta_e j})^2 \boldsymbol{s}_j \boldsymbol{s}_j^H + (\boldsymbol{n}_{\Sigma} - \boldsymbol{n}_{\Delta_e})(\boldsymbol{n}_{\Sigma} - \boldsymbol{n}_{\Delta_e})^H]}. \tag{41}$$

3.4. Principle of the Algorithm in This Paper

In practice, the received signal $\boldsymbol{X}$ of the monopulse antenna can be obtained by measurement. To ensure the maximization of the *EIF*, consider the inter-beam spatial filtering for the received signal $\boldsymbol{X}$, set the spatial filter as $\boldsymbol{w}$, and

$$\boldsymbol{g}_t = \begin{bmatrix} g_{\Sigma t} \\ g_{\Delta_e t} \\ g_{\Delta_a t} \\ g_{\Delta_\Delta t} \end{bmatrix} \tag{42}$$

is the target signal gain vector; the four elements in the vector are the gain values of the four radar channels with respect to the target signal.

To solve the spatial filter $\boldsymbol{w}$, the following optimization model is established based on the *EIF* maximization design criterion:

$$\begin{cases} \min \boldsymbol{w}^H \boldsymbol{X} \boldsymbol{X}^H \boldsymbol{w} \\ \text{s.t.} \quad \boldsymbol{w}^H \boldsymbol{g}_t = 1 \end{cases}, \tag{43}$$

where $\min(\cdot)$ is for finding the minimum of $(\cdot)$, and s.t.$(\cdot)$ represents the constraint conditions.

$\boldsymbol{XX}^H$ represents the power of the signal received by the radar, and $\boldsymbol{w}^H\boldsymbol{XX}^H\boldsymbol{w}$ represents the power of the signal received after filtering. Since the jamming power is much larger than the sum of the power of the target signal and the noise, the jamming power is similar to the power of the mixed signal received by the radar. The gain vector of the target signal is kept constant through constraints, that is, the power of the target signal is unchanged. In this case, when the filtered received signal power is the minimum value, the jamming power is the minimum, so the *EIF* is always the maximum value.

When applying the Lagrange multiplier method to solve the model, set

$$\xi = \boldsymbol{w}^{\mathrm{H}}\boldsymbol{X}\boldsymbol{X}^{\mathrm{H}}\boldsymbol{w} + \lambda\left(\boldsymbol{w}^{\mathrm{H}}\boldsymbol{g}_{\mathrm{t}} - 1\right), \tag{44}$$

and then we have $\frac{\partial \xi}{\partial \boldsymbol{w}^{\mathrm{H}}} = \boldsymbol{X}\boldsymbol{X}^{\mathrm{H}}\boldsymbol{w} + \lambda\boldsymbol{g}_{\mathrm{t}}$, and we can obtain $\boldsymbol{w}$ after setting it to zero

$$\boldsymbol{w} = -\lambda(\boldsymbol{X}\boldsymbol{X}^{\mathrm{H}})^{-1}\boldsymbol{g}_{\mathrm{t}}. \tag{45}$$

Substituting (45) into the constraints of (43), we obtain

$$\lambda = -\frac{1}{\boldsymbol{g}_{\mathrm{t}}^{\mathrm{H}}(\boldsymbol{X}\boldsymbol{X}^{\mathrm{H}})^{-1}\boldsymbol{g}_{\mathrm{t}}}. \tag{46}$$

Therefore,

$$\boldsymbol{w} = -\frac{(\boldsymbol{X}\boldsymbol{X}^{\mathrm{H}})^{-1}\boldsymbol{g}_{\mathrm{t}}}{\boldsymbol{g}_{\mathrm{t}}^{\mathrm{H}}(\boldsymbol{X}\boldsymbol{X}^{\mathrm{H}})^{-1}\boldsymbol{g}_{\mathrm{t}}}, \tag{47}$$

and then the output signal after spatial filtering is

$$\boldsymbol{S}=\boldsymbol{w}^{\mathrm{H}}\boldsymbol{X}. \tag{48}$$

The *SJNR* of the filtered output signal $\boldsymbol{S}$ will take the maximum value in the incoming direction of the target when the direction of the jamming remains unchanged. Therefore, to ensure that the constraint direction is the target direction, the 3 dB beamwidth is used as the search range of the target incoming pitch angle θ_{et} and azimuth angle θ_{bt}, and the points of m and n are taken at equal intervals within the search range.

$$\theta_{\mathrm{etm}} = \theta_{\mathrm{et0}} + m\Delta\theta_{\mathrm{et}}, \tag{49}$$

$$\theta_{\mathrm{btn}} = \theta_{\mathrm{bt0}} + n\Delta\theta_{\mathrm{bt}}. \tag{50}$$

where θ_{et0} and θ_{bt0} are the starting search angles of the pitch angle and azimuth angle, respectively, and $\Delta\theta_{\mathrm{et}}$ and $\Delta\theta_{\mathrm{bt}}$ are the search angle steps of the pitch angle and azimuth angle, respectively. In each search direction, the corresponding spatial filter is formed, and the *SJNR* of the filtered output signal in that direction is calculated. The direction corresponding to the largest *SJNR* is the target direction, and the spatial filter is formed in that direction to filter the echo signal for target detection.

The algorithm in this paper requires target detection after filtering the echo signal. To facilitate representation, set

$$\boldsymbol{w} = -\frac{(\boldsymbol{X}\boldsymbol{X}^{\mathrm{H}})^{-1}\boldsymbol{g}_{\mathrm{t}}}{\boldsymbol{g}_{\mathrm{t}}^{\mathrm{H}}(\boldsymbol{X}\boldsymbol{X}^{\mathrm{H}})^{-1}\boldsymbol{g}_{\mathrm{t}}} = \begin{bmatrix} w_1 \\ w_2 \\ w_3 \\ w_4 \end{bmatrix}, \tag{51}$$

then

$$\boldsymbol{S}=\boldsymbol{w}^{\mathrm{H}}\boldsymbol{X}=w_1\boldsymbol{x}_{\Sigma}+w_2\boldsymbol{x}_{\Delta_{\mathrm{e}}}+w_3\boldsymbol{x}_{\Delta_{\mathrm{a}}}+w_4\boldsymbol{x}_{\Delta_{\Delta}}. \tag{52}$$

Therefore, the power of the target signal, jamming, and noise when using the algorithm in this paper for target detection is

$$P_{\mathrm{t}}=(w_1g_{\Sigma\mathrm{t}}+w_2g_{\Delta_{\mathrm{e}}\mathrm{t}}+w_3g_{\Delta_{\mathrm{a}}\mathrm{t}}+w_4g_{\Delta_{\Delta}\mathrm{t}})^2\boldsymbol{s}_{\mathrm{t}}\boldsymbol{s}_{\mathrm{t}}^{\mathrm{H}}, \tag{53}$$

$$P_{\mathrm{j}}=(w_1g_{\Sigma\mathrm{j}}+w_2g_{\Delta_{\mathrm{e}}\mathrm{j}}+w_3g_{\Delta_{\mathrm{a}}\mathrm{j}}+w_4g_{\Delta_{\Delta}\mathrm{j}})^2\boldsymbol{s}_{\mathrm{j}}\boldsymbol{s}_{\mathrm{j}}^{\mathrm{H}}, \tag{54}$$

$$P_{\mathrm{n}}=w_1^2\boldsymbol{n}_{\Sigma}\boldsymbol{n}_{\Sigma}^{\mathrm{H}}+w_2^2\boldsymbol{n}_{\Delta_{\mathrm{e}}}\boldsymbol{n}_{\Delta_{\mathrm{e}}}^{\mathrm{H}}+w_3^2\boldsymbol{n}_{\Delta_{\mathrm{a}}}\boldsymbol{n}_{\Delta_{\mathrm{a}}}^{\mathrm{H}}+w_4^2\boldsymbol{n}_{\Delta_{\Delta}}\boldsymbol{n}_{\Delta_{\Delta}}^{\mathrm{H}}. \tag{55}$$

From (53)–(55), the *SJNR* of the algorithm in this paper is

$$SJNR_{\mathrm{NEW}}=\frac{(w_1g_{\Sigma\mathrm{t}}+w_2g_{\Delta_{\mathrm{e}}\mathrm{t}}+w_3g_{\Delta_{\mathrm{a}}\mathrm{t}}+w_4g_{\Delta_{\Delta}\mathrm{t}})^2\boldsymbol{s}_{\mathrm{t}}\boldsymbol{s}_{\mathrm{t}}^{\mathrm{H}}}{(w_1g_{\Sigma\mathrm{j}}+w_2g_{\Delta_{\mathrm{e}}\mathrm{j}}+w_3g_{\Delta_{\mathrm{a}}\mathrm{j}}+w_4g_{\Delta_{\Delta}\mathrm{j}})^2\boldsymbol{s}_{\mathrm{j}}\boldsymbol{s}_{\mathrm{j}}^{\mathrm{H}}+(w_1^2\boldsymbol{n}_{\Sigma}\boldsymbol{n}_{\Sigma}^{\mathrm{H}}+w_2^2\boldsymbol{n}_{\Delta_{\mathrm{e}}}\boldsymbol{n}_{\Delta_{\mathrm{e}}}^{\mathrm{H}}+w_3^2\boldsymbol{n}_{\Delta_{\mathrm{a}}}\boldsymbol{n}_{\Delta_{\mathrm{a}}}^{\mathrm{H}}+w_4^2\boldsymbol{n}_{\Delta_{\Delta}}\boldsymbol{n}_{\Delta_{\Delta}}^{\mathrm{H}})}, \tag{56}$$

so the *EIF* of the algorithm in this paper is

$$\begin{aligned}EIF_{\mathrm{NEW}}&=\frac{SJNR_{\mathrm{NEW}}}{SJNR_0}\\&=\frac{(w_1g_{\Sigma\mathrm{t}}+w_2g_{\Delta_{\mathrm{e}}\mathrm{t}}+w_3g_{\Delta_{\mathrm{a}}\mathrm{t}}+w_4g_{\Delta_{\Delta}\mathrm{t}})^2[(g_{\Sigma\mathrm{j}})^2\boldsymbol{s}_{\mathrm{j}}\boldsymbol{s}_{\mathrm{j}}^{\mathrm{H}}+\boldsymbol{n}_{\Sigma}\boldsymbol{n}_{\Sigma}^{\mathrm{H}}]}{(g_{\Sigma\mathrm{t}})^2[(w_1g_{\Sigma\mathrm{j}}+w_2g_{\Delta_{\mathrm{e}}\mathrm{j}}+w_3g_{\Delta_{\mathrm{a}}\mathrm{j}}+w_4g_{\Delta_{\Delta}\mathrm{j}})^2\boldsymbol{s}_{\mathrm{j}}\boldsymbol{s}_{\mathrm{j}}^{\mathrm{H}}+(w_1^2\boldsymbol{n}_{\Sigma}\boldsymbol{n}_{\Sigma}^{\mathrm{H}}+w_2^2\boldsymbol{n}_{\Delta_{\mathrm{e}}}\boldsymbol{n}_{\Delta_{\mathrm{e}}}^{\mathrm{H}}+w_3^2\boldsymbol{n}_{\Delta_{\mathrm{a}}}\boldsymbol{n}_{\Delta_{\mathrm{a}}}^{\mathrm{H}}+w_4^2\boldsymbol{n}_{\Delta_{\Delta}}\boldsymbol{n}_{\Delta_{\Delta}}^{\mathrm{H}})]}.\end{aligned} \tag{57}$$

4. Experimental Simulation

In this paper, the experimental simulation uses a monopulse radar with 80 × 80 array elements that are half-wavelength spaced. The azimuth dimension and pitch dimension antenna beam pointing values are 0°, both search ranges are 1°, both search angle steps are 0.05°, and both 3 dB beamwidths are 1°, with the jamming coming from the pitch angle −0.2° and azimuth angle −0.3°.

4.1. Experimental Simulation of the EIF of the Algorithm

Under the above conditions, the Signal-to-Noise Ratio (SNR) is 20 dB, the EIFs of the algorithms in different target signal directions are calculated with different SJR values. The pitch and azimuth angles of the target signals are in the range of −0.5° to 0.5°, and both angle steps are 0.05°. In total, 1000 Monte Carlo simulation experiments were conducted at each angle to calculate the *EIF*, and the average value was taken as the *EIF* of the algorithm in the direction of the target signal. Because modern jammers usually require the SJR of radar systems to be less than −10 dB and since the object of this paper is main-lobe jamming, SJR will be lower, so SJR is set as −30 dB, −50 dB, and −70 dB in this paper. Figure 3 shows the EIF of the algorithm as a function of the target angle when SJR is −50 dB.

As can be seen in Figure 3, the *EIF* of the MLC algorithm after azimuth dimension jamming cancellation varies greatly with the azimuth angle of the target and only slightly with the pitch angle of the target. Therefore, in order to better compare the EIFs of the algorithms, three target pitch angles were selected to observe the variation in the *EIF* with the target azimuth angle. The three target pitch angles are the target pitch angle at a distance of 1/3 and 2/3 of the beamwidth from the jamming and the angle at the same angle as the jamming pitch angle. The *EIF* of the MLC algorithm after azimuth dimension jamming cancellation was compared with that of the proposed algorithm. Figure 4 shows the simulation results, where (a), (b), and (c) are the curves of the *EIF* with the target azimuth angle under different SJR values when the target pitch angle is −0.2°, 0.15°, and 0.5°, respectively.

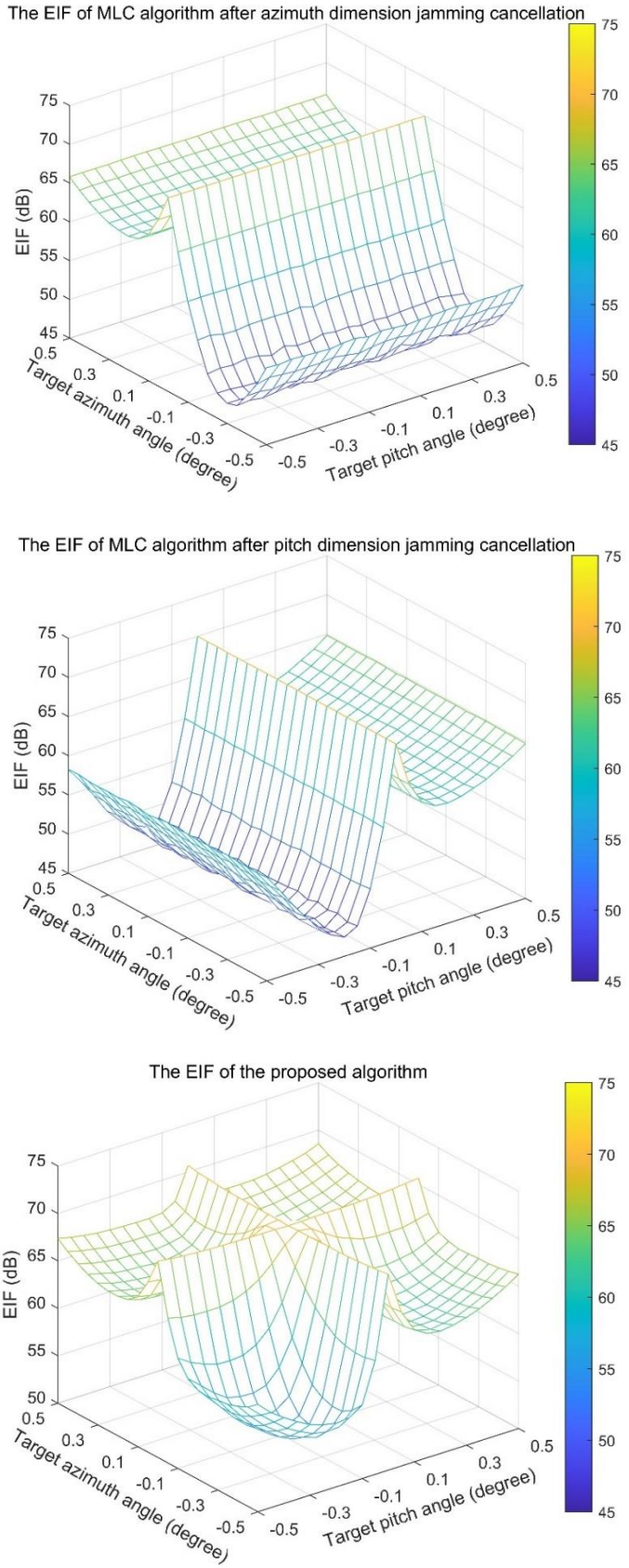


Figure 3. The EIF of two algorithms when the SJR is −50 dB.

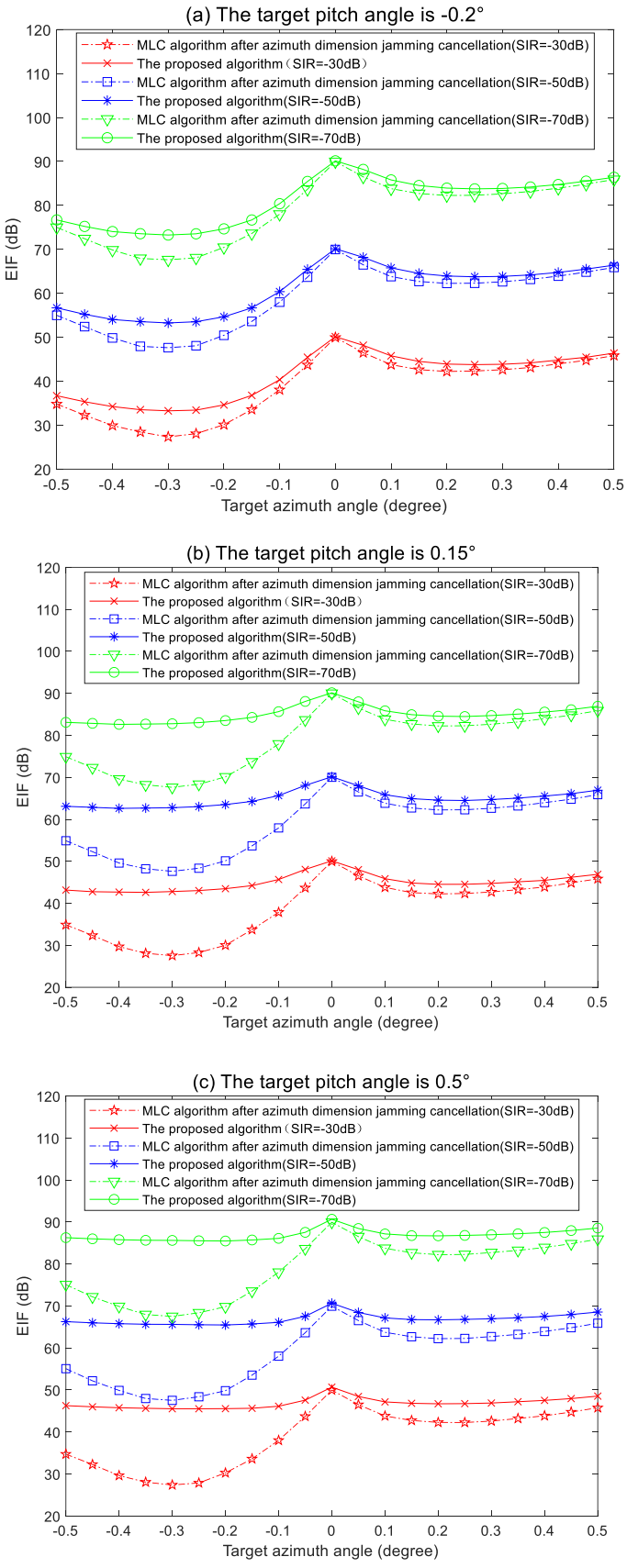


Figure 4. The EIFs of the two algorithms.

It can be seen from Figure 4 that when the target pitch angle is -0.2°, that is, the target pitch angle is equal to the jamming pitch angle (as shown in a of Figure 4), the variation trend of the *EIF* of the two algorithms with the target azimuth angle is basically the same. When the target pitch angle is 0.15° or 0.5°, that is, the target pitch angle is not equal to the jamming pitch angle (as shown in b and c of Figure 4), and the target azimuth angle ranges from 0° to 0.5°, the *EIF* of the proposed algorithm is slightly higher than that of the MLC algorithm after azimuth dimension jamming cancellation.

Similarly, the *EIF* of the MLC algorithm after pitch dimension jamming cancellation varies greatly with the pitch angle of the target and only slightly with the azimuth angle of the target. Therefore, three target azimuth angles were selected to observe the variation of the *EIF* with the target pitch angle: the target azimuth angle at a distance of 1/3 and 2/3 of the beamwidth from the jamming and the angle at the same angle as the jamming azimuth angle, and the *EIF* of the MLC algorithm after pitch dimension jamming cancellation was compared with that of the proposed algorithm. Figure 5 shows the simulation results, where (a), (b), and (c) are the curves of the *EIF* with the target pitch angle under different SJR values when the target azimuth angle is -0.3°, 0.05°, and 0.4°, respectively.

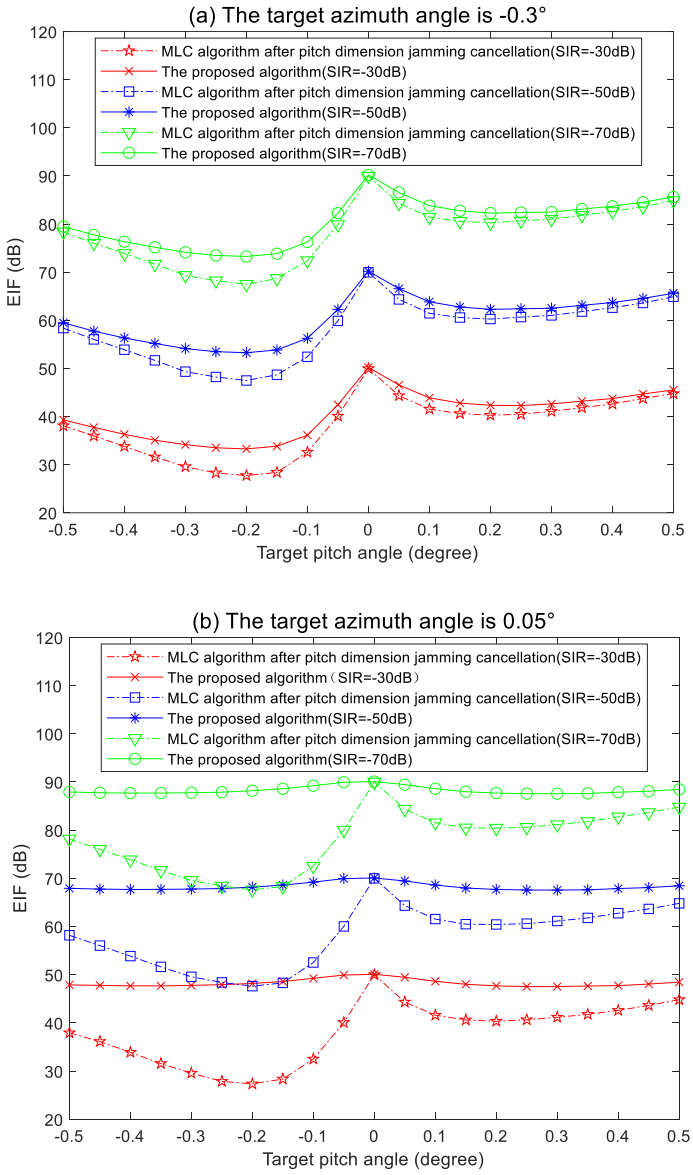


Figure 5. *Cont*.

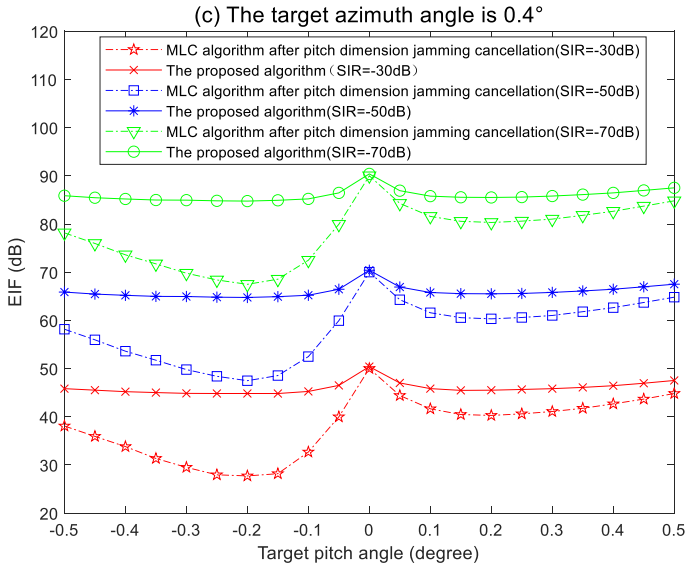


Figure 5. The EIFs of the two algorithms.

As can be seen in Figure 5, the variation trend of the *EIF* of the algorithm in this paper and that of the MLC algorithm after pitch dimension jamming cancellation with the change in the target pitch angle is basically consistent with the variation trend of the *EIF* of the algorithm in this paper and with that of the MLC algorithm after azimuth dimension jamming cancellation with the change in the target azimuth angle shown in Figure 4.

4.2. Experimental Simulation of the Algorithm Detection Performance

To further study the detection performance of the algorithms, the target angle step was set to 0.05° in the pitch dimension and azimuth dimension. In total, 1000 Monte Carlo experimental simulations were performed on each angle, and the CA-CFAR technique was used for target detection; the number of target echo points was set as 2000, the number of reference cells as 20, the number of protection cells as 6, and the false alarm probability as 1×10^{-6}. The detection probabilities of the two algorithms under different SJR values at different target angles were calculated. Figure 6 shows the variation trend of the detection probability of the two algorithms with the target angle when the SJR is -50 dB.

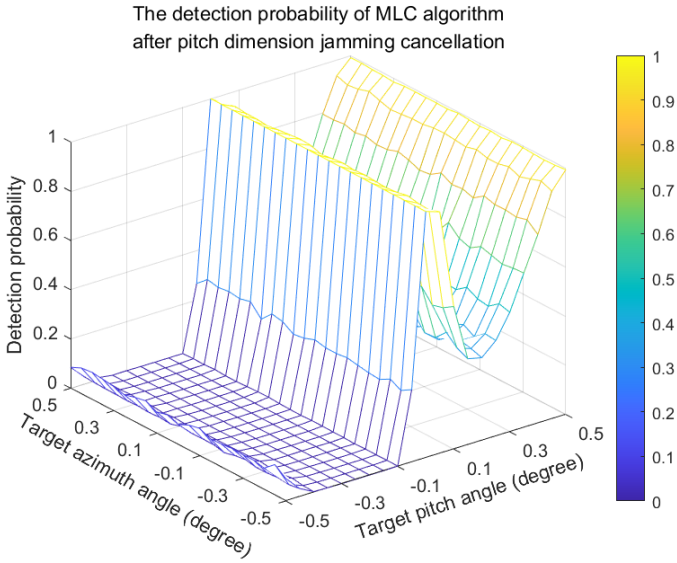


Figure 6. *Cont.*

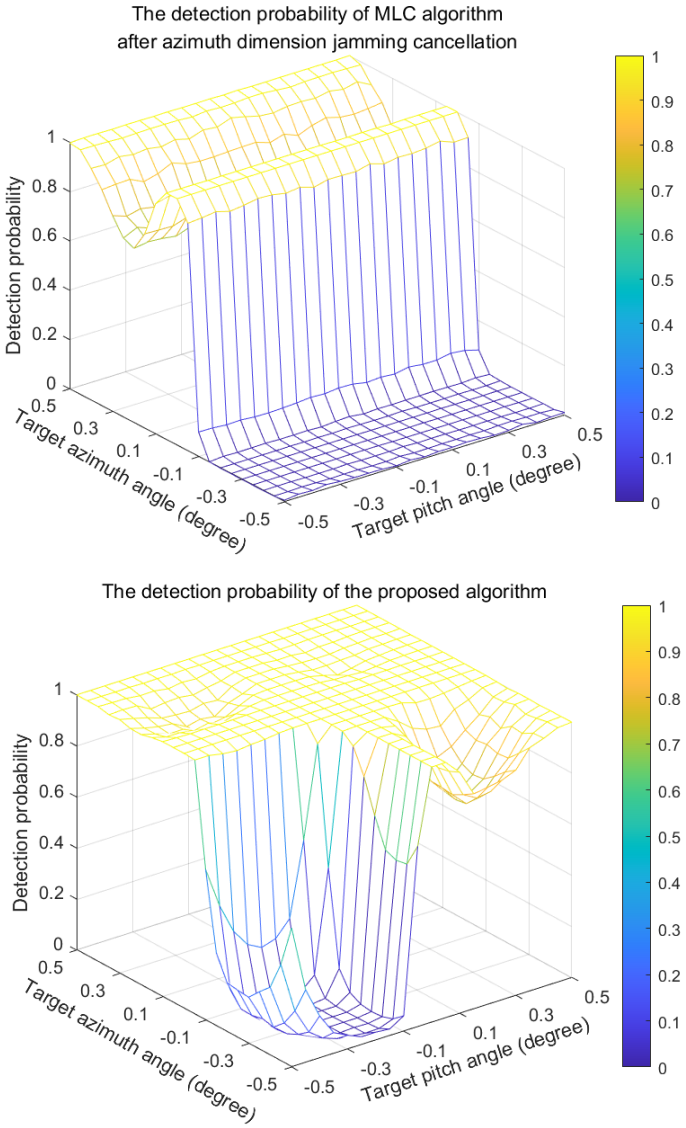


Figure 6. The detection probabilities of the two algorithms when the SJR is −50 dB.

Similarly, when the target pitch angle is −0.2°, 0.15°, and 0.5°, the detection probability of the MLC algorithm after azimuth dimension jamming cancellation was compared with that of the proposed algorithm. When the target azimuth angle was −0.3°, 0.05°, and 0.4°, the detection probability of the MLC algorithm after pitch dimension jamming cancellation was compared with that of the proposed algorithm. Figures 7 and 8 show the simulation results; Figure 7a–c represents the curves of the detection probability of the two algorithms with different SJR values when the target pitch angle is −0.2°, 0.15°, and 0.5°, respectively. Figure 8a–c represents the curves of the target azimuth angle when the target azimuth angle is −0.3°, 0.05°, and 0.4°, respectively. The curve of the detection probability with the target pitch angle was determined under different SJR values using the two algorithms.

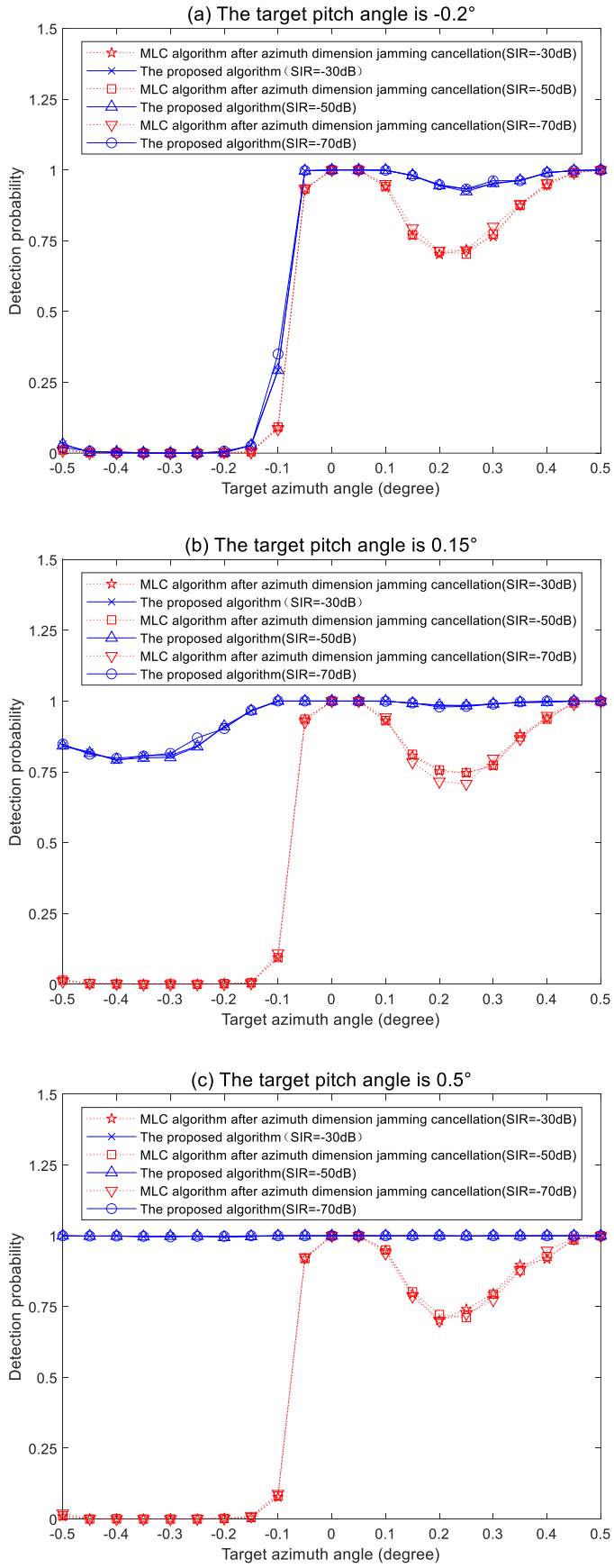


Figure 7. The detection performance of the two algorithms.

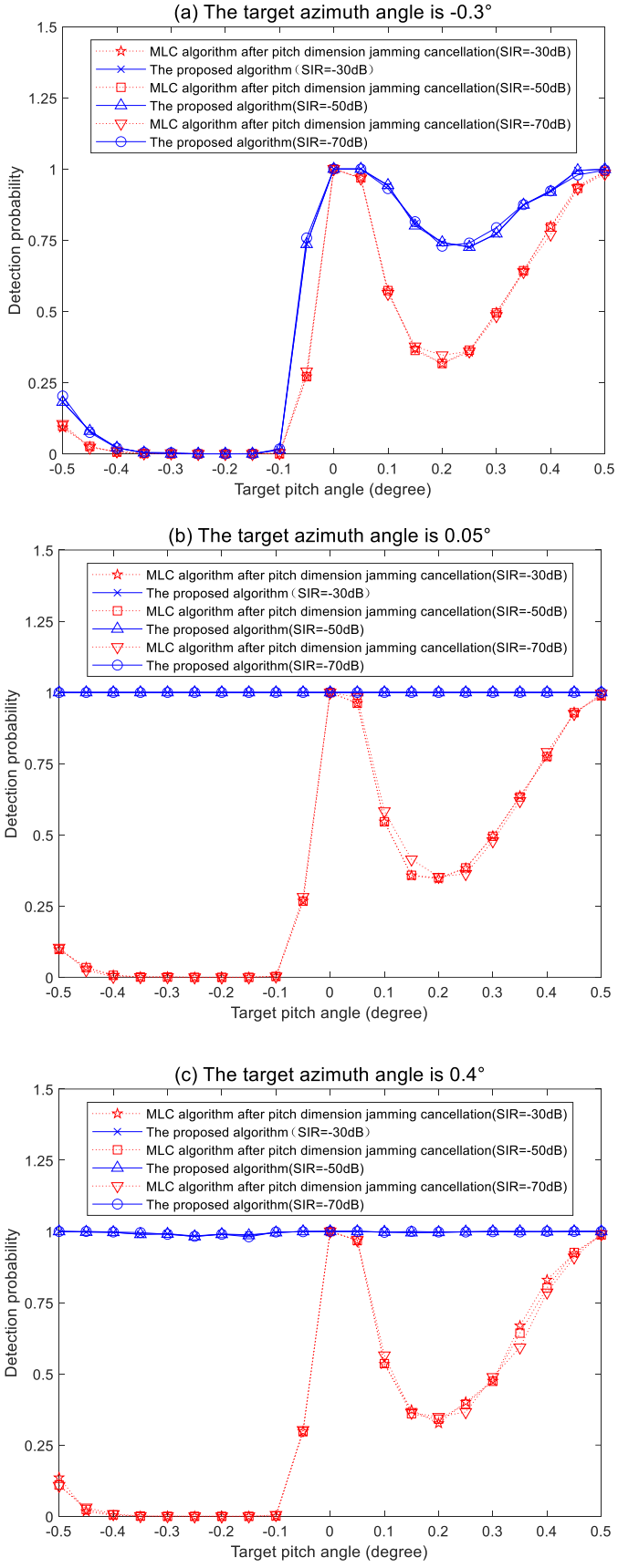


Figure 8. The detection performance of the two algorithms.

As can be seen in Figure 7, both algorithms had good detection performance when the target azimuth angle was near 0°. When the target azimuth angle was between −0.5° and −0.1°, the detection probability of the MLC algorithm after azimuth dimension jamming cancellation was basically 0 due to the small spacing with the jamming, while the target pitch angle of the proposed algorithm was −0.2°, that is, the target pitch angle was equal to the jamming pitch angle (as shown in a of Figure 7), and the detection performance of the proposed algorithm was basically the same as that of the MLC algorithm after azimuth dimension jamming cancellation. However, when the target pitch angle was 0.15° or 0.5°, that is, the target pitch angle was not equal to the jamming pitch angle (as shown in b and c of Figure 7), the detection performance of the proposed algorithm was significantly better than that of the MLC algorithm after azimuth dimension jamming cancellation. When the target azimuth angle was between 0.1° and 0.5°, the detection probability of both algorithms exceeded 0.6, but the detection performance of the proposed algorithm was better than that of the MLC algorithm after azimuth dimension jamming cancellation.

As can be seen in Figure 8, the variation trend of the detection performance of the algorithm in this paper and the MLC algorithm after pitch dimension jamming cancellation with the change in the target pitch angle was basically consistent with the variation trend of the detection performance of the algorithm in this paper and the MLC algorithm after azimuth dimension jamming cancellation with the change in the target azimuth angle shown in Figure 7.

5. Discussion

The algorithm in this paper utilizes the received signal of four channels, which is less affected by the jamming residuals, while the MLC monopulse algorithm uses the pitch difference channel or azimuth difference channel to eliminate the jamming in the sum channel, which only utilizes two channel signals and is more affected by the jamming residuals. Therefore, the detection performance of the algorithm in this paper is better.

6. Conclusions

In this paper, a target detection algorithm for monopulse radar in the case of main-lobe cover jamming is proposed, which ensures that the filtered target echo EIF is maximized by searching for the direction within the main lobe where the *SJNR* of the echo signal takes the maximum value and by adaptively forming an inter-beam spatial filter in that direction.

Author Contributions: Conceptualization, Q.Z.; methodology, L.W. and Q.Z.; Writing—Original Draft, L.W.; writing—review and editing, L.W. and P.W. All authors have read and agreed to the published version of the manuscript.

Funding: This research received no external funding.

Data Availability Statement: Data are available on request from the authors.

Acknowledgments: The authors thank for the valuable and constructive comments from the editor and reviewers.

Conflicts of Interest: The authors declare no conflict of interest.

References

1. Sherman, S.M.; Barton, D.K. *Monopulse Principles and Techniques*; Artech House: Washington, DC, USA, 2011.
2. Bayderkhani, R.; Hassani, H.R. Very-low-sidelobe printed tapered arc-shaped wide-slot antenna array. *Iet Microw. Antennas Propag.* **2011**, *5*, 1143–1147. [CrossRef]
3. Chopra, R.; Kumar, G. Series-Fed Binomial Microstrip Arrays for Extremely Low Sidelobe Level. *IEEE Trans. Antennas Propag.* **2019**, *67*, 4275–4279. [CrossRef]
4. Howells, P.W. Intermediate Frequency Side-Lobe Canceller. U.S. Patent US3202990 A, 24 August 1965.
5. Applebaum, S.; Chapman, D. Adaptive arrays with main beam constraints. *Antennas Propag. IEEE Trans. Antennas Propag.* **1976**, *24*, 650–662. [CrossRef]
6. El-Azhary, I.; Afifi, M.S.; Excell, P.S. A simple algorithm for sidelobe cancellation in a partially adaptive linear array. *IEEE Trans. Antennas Propag.* **1988**, *36*, 1482–1486. [CrossRef]

7. Vendik, O.G.; Kozlov, D.S. Phased Antenna Array with a Sidelobe Cancellation for Suppression of Jamming. *IEEE Antennas Wirel. Propag. Lett.* **2012**, *11*, 648–650. [CrossRef]
8. Tian, H. Design of an Adaptive Sidelobe Cancellation Algorithm for Radar. In *Journal of Physics: Conference Series*; No. 1; IOP Publishing: Bristol, UK, 2021; Volume 1754.
9. O'Sullivan, M.R. A comparison of sidelobe blanking systems. In Proceedings of the Radar-87: International Conference, London, UK, 19–21 October 1987.
10. Shnidman, D.A.; Toumodge, S.S. Sidelobe blanking with integration and target fluctuation. *IEEE Trans. Aerosp. Electron. Syst.* **2002**, *38*, 1023–1037. [CrossRef]
11. Maisel, L. Performance of Sidelobe Blanking Systems. *IEEE Trans. Aerosp. Electron. Syst. AES* **1968**, *4*, 174–180. [CrossRef]
12. Haimovich, A.M.; Bar-Ness, Y. An eigenanalysis interference canceler. *IEEE Trans. Signal Process.* **2002**, *39*, 76–84. [CrossRef]
13. Yu, S.J.; Lee, J.H. Efficient eigenspace-based array signal processing using multiple shift-invariant subarrays. *IEEE Trans. Antennas Propag.* **2002**, *47*, 186–194.
14. Yang, J.; Liu, C. Improved Mainlobe Interference Suppression Based on Blocking Matrix Preprocess. *J. Electr. Comput. Eng.* **2015**, *2015*, 1–8. [CrossRef]
15. Chen, X.; Shu, T.; Yu, K.-B.; He, J.; Yu, W. Joint Adaptive Beamforming Techniques for Distributed Array Radars in Multiple Mainlobe and Sidelobe Jammings. *IEEE Antennas Wirel. Propag. Lett.* **2019**, *19*, 248–252. [CrossRef]
16. Yang, X.; Zhang, Z.; Zeng, T.; Long, T.; Sarkar, T.K. Mainlobe Interference Suppression Based on Eigen-Projection Processing and Covariance Matrix Reconstruction. *IEEE Antennas Wirel. Propag. Lett.* **2014**, *13*, 1369–1372. [CrossRef]
17. Lu, L.; Liao, Y. Improved algorithm of mainlobe interference suppression based on eigen-subspace. In Proceedings of the 2016 International Conference on Communication and Signal Processing (ICCSP) IEEE, Melmaruvathur, India, 6–8 April 2016.
18. Luo, Z.; Wang, H.; Lv, W.; Tian, H. Mainlobe Anti-Jamming via Eigen-Projection Processing and Covariance Matrix Reconstruction. *IEICE Trans. Fundam. Electron. Commun. Comput. Sci. E* **2017**, *100*, 1055–1059. [CrossRef]
19. Yu, K.B.; Murrow, D.J. Adaptive digital beamforming for angle estimation in jamming. *IEEE Trans. Aerosp. Electron. Syst.* **2002**, *37*, 508–523.
20. Li, R.; Rao, C.; Dai, L.; Wang, Y. Combining sum-difference and auxiliary beams for adaptive monopulse in jamming. *J. Syst. Eng. Electron.* **2013**, *24*, 372–381. [CrossRef]
21. Chernyak, V.S. Adaptive mainlobe jamming cancellation and target detection in multistatic radar systems. In Proceedings of the Radar, Cie International Conference of 0, Beijing, China, 8–10 October 1996.
22. Xia, D.P.; Zhang, L.; Wu, T.; Meng, X.-D. A Mainlobe Interference Suppression Algorithm Based on Bistatic Airborne Radar Cooperation. In Proceedings of the 2019 IEEE Radar Conference (RadarConf19) IEEE, Boston, MA, USA, 22–26 April 2019.
23. Ge, M.; Cui, G.; Yu, X.; Kong, L. Mainlobe jamming suppression with polarimetric multi-channel radar via independent component analysis. *Digit. Signal Process.* **2020**, *106*, 102806. [CrossRef]
24. Schuerger, J.; Garmatyuk, D. Performance of random OFDM radar signals in deception jamming scenarios. In Proceedings of the Radar Conference IEEE, Pasadena, CA, USA, 4–8 May 2009.
25. Greco, M.; Gini, F.; Farina, A. Radar Detection and Classification of Jamming Signals Belonging to a Cone Class. *IEEE Trans. Signal Process.* **2008**, *56*, 1984–1993. [CrossRef]
26. Ayub, A.; Sabir, Z.; Altamirano, G.C.; Sadat, R.; Ali, M.R. Characteristics of melting heat transport of blood with time-dependent cross-nanofluid model using Keller–Box and BVP4C method. *Eng. Comput.* **2022**, *38*, 3705–3719. [CrossRef]
27. Umar, M.; Amin, F.; Al-Mdallal, Q.; Ali, M.R. A stochastic computing procedure to solve the dynamics of prevention in HIV system. *Biomed. Signal Process. Control* **2022**, *78*, 103888. [CrossRef]
28. Finn, H.M.; Johnson, R.S. Adaptive Detection Mode with Threshold Control as a Function of Spatially Sampled Clutter-Level Estimates. *Rca Rev.* **1968**, *29*, 414–463.
29. Johnston S, L. The ECCM improvement factor (EIF)-Illustrative examples, applications, and considerations in its utilization in radar ECCM performance assessment. *Int. Conf. Radar.* **1986**, 149–154.